15 Calendering

15.1 THE CALENDERING PROCESS

Two-roll mills and calenders belong to the earliest group of equipment used for processing natural rubber. They were introduced in the 1830s by Edwin Chaffee and Charles Goodyear in the United States, as described in Section 1.1. The number of rolls of a calender is determined by the nature of material processed and the product. Rubber can be calendered on a two-roll calender, with four-roll calenders generally used for double coating of substrates [Fig. 15.1(a)]. However, the surface quality requirements of calendered thermoplastic polymer require four-roll calenders [Figs. 15.1(b), 15.1(c)]. Therefore, when calendaring polymers, the material passes three nip regions. The first pass is the "feed" pass, the second, the "metering" pass, and the third, the "sheet formation, gauging, and finishing" pass (1). Calenders with five rolls in various arrangements are also used.

Transfer from one roll to the next is accomplished by some combination of differentials in roll speed, temperature, and surface finish (2). The width of the sheet (when the speed of both rolls is equal) changes at each nip in inverse proportion to the decrease in thickness. The production rate of a calendering line, when not limited by the mixing and melting capacity upstream, is determined primarily by the size and surface requirements of the product and the properties of the polymer (1). Thus, heavy sheets of 0.25 mm and up can be produced at 60 m/min without difficulty. Even higher speeds are possible if the sheet is posttreated (e.g., embossed, top coated). However, certain rigid, glossy, roller-polished sheets are produced at much lower rates of 10–35 m/min. Thin flexible films can be produced at 100 m/min at the roll and 125 m/min at the winder. The higher speed at the winder is due to a drawdown process that helps in producing thin films (0.04 mm and below); films of such thickness would be hard to separate from the roll.

Calender sizes range up to 90 cm (36 in) in diameter and 250 cm (97 in) wide, with polymer throughputs up to 4000 kg/h. The surface temperature of the rolls is carefully controlled by using drilled rolls—that is, axially drilled holes all around the periphery—in which a temperature-controlling liquid is circulated.

The calendering process is commonly used for shaping high melt viscosity thermoplastic sheets and is particularly suitable for polymers susceptible to thermal degradation or containing substantial amounts of solid additives. This is because the calender can convey large rates of melt with a small mechanical energy input (compared to an extruder).

Principles of Polymer Processing, Second Edition, by Zehev Tadmor and Costas G. Gogos

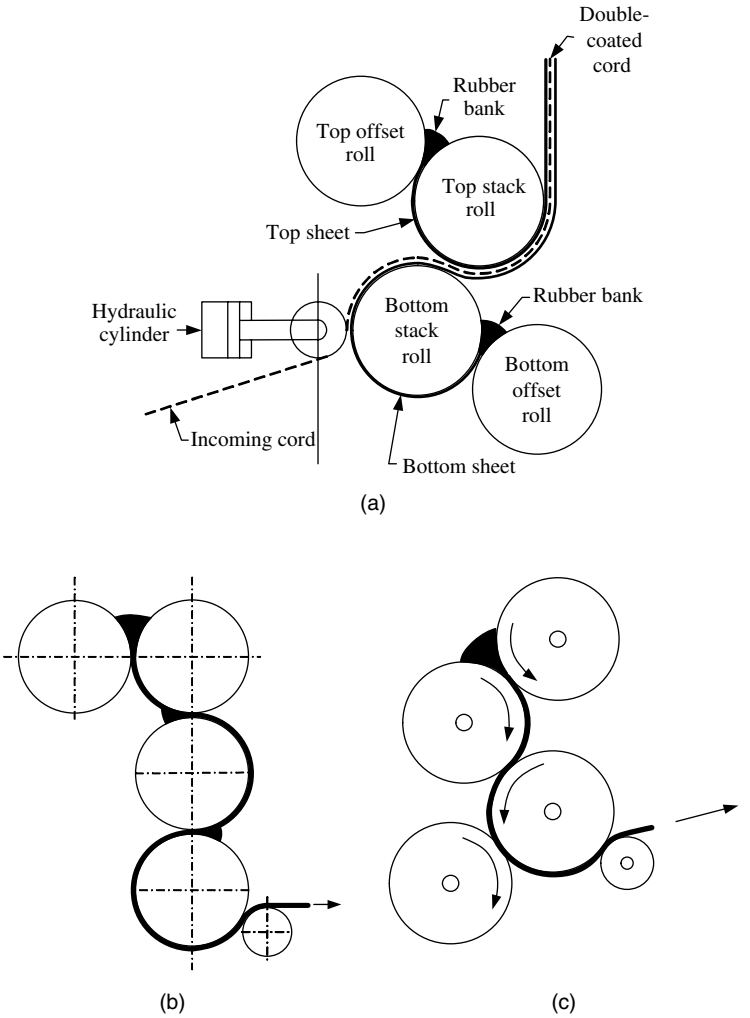

Fig. 15.1 (a) A four-roll, inclined "Z" calender for double casting of tire cord. (b) A four-roll, inverted "L" calender. (c) A four-roll "Z" calender.

The thickness of the calendered product must be uniform in both the machine and cross-machine directions. Any variation in gap size due to roll dimensions, setting, thermal effects, and roll distortion due to high pressures developing in the gap, will result in product nonuniformity in the cross-machine direction. Eccentricity of the roll with respect to the roll shaft, as well as roll vibration and feed uniformity, must be tightly controlled to avoid nonuniformity in the machine direction. A uniform empty gap size will be distorted in operation because of hydrodynamic forces, developed in the nip, which deflect the rolls. The resulting product from such a condition will be thick in the middle and thin at the edges, as shown in Fig. 15.2.

Three common methods, which are commonly referred to as *roll-crown*, *roll-crossing*, and *roll-bending*, are employed to compensate for this deformation. Roll-crown indicates that the roll diameter at the center is slightly greater than at the edges. In principle, by applying an appropriate roll diameter and profile, roll deflection can be exactly

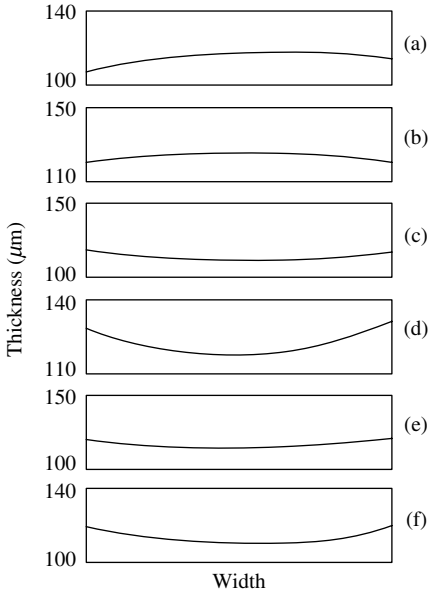

Fig. 15.2 Effect of roll-crossing and -bending on web uniformity in a calender 1.8 m wide. (a) No crossing or bending. (b) Crossing, 4 mm; no bending. (c) Crossing, 8 mm; no bending. (d) Crossing, 12 mm; no bending. (e) No crossing, bending of 10 Mp. (f) No crossing, bending of 16 Mp. [Reprinted by permission from D. Katz, "An Inquiry on the Behavior of Bingham Materials in Calender Processing," M. S. Thesis, Department of Mechanics, Technion—Israel Institute of Technology, Haifa, 1973.]

compensated for *given* operating conditions. Roll-crossing and roll-bending provide means for continuous adjustment of gap size distribution. Roll-crossing results in a wider gap at the edges and can easily be visualized as giving the same effect as increasing the roll-crown. In roll-bending, a bending moment is applied on both ends of the roll by two additional bearings, which can increase or decrease the bending due to hydrodynamic forces.

Figure 15.2 shows the effect of roll-crossing and roll-bending on product uniformity. An exact knowledge of the hydrodynamic pressure distribution in the nip is therefore necessary for predicting by structural analysis the exact gap thickness distribution, as well as the load on the bearings; we discuss this in Section 15.4. Accurate gap thickness control and stringent roll temperature uniformity requirements are indicative of the sensitivity of the product quality to minor variations in conditions. It is not surprising, therefore, that a calender line takes a long time, sometimes hours, to "stabilize," that is, to reach steady state. Consequently calender lines are best utilized in long production runs. The ruggedness and basic simplicity of the machine elements involved are fully compatible with such long runs.

15.2 MATHEMATICAL MODELING OF CALENDERING

A comprehensive mathematical model of the calendering process should consist of a coupled hydrodynamic and roll structural analysis, heat transfer in the deforming polymer

and the rolls, and product response to drawdown. By taking into account the rheological properties of the material, feed conditions, and operating conditions, such as roll speeds and temperatures, gap separation, roll-crossing and -bending, the following matters can be ascertained: the exact nature of the flow in the nip, the width variation from nip to nip, and the thickness and temperature distribution, as well as the effect of these conditions on the transfer of the material from roll to roll, and the onset of instabilities. Such a model would assist the calender designer in selecting roll size, gap separation, roll-crown, -crossing, and -bending requirements, and operating conditions for given production rates and quality requirements.

The first step in developing such a model (cf. Section 6.4) is to gain a clear *qualitative* picture on the exact nature of the flow mechanism. A viscoelastic melt is fed into the first nip in strips. The melt accumulates in the center zone of the nip area and simultaneously undergoes flow into the nip and sideways; the drag-induced flow leads to pressure buildup, which inevitably produces pressure gradients in the machine and cross-machine directions, resulting in the flow above. Experimental evidence of such a pressure distribution is given by Unkrüer (3), who reports on detailed calendering studies of polyvinyl chloride (PVC) and polystyrene (PS).

Figure 15.3 gives pressure profiles at three cross-machine locations. Thus, a complex three-dimensional flow field is set up with an a priori, unspecified free boundary. Axial flow (cross-machine direction) continues throughout the nip zone all the way to the exit, but the rate varies because of the varying gap size. That is, in the narrow region of the nip, drag flow in the direction of rotation is predominant as compared to cross-machine pressure flow.

According to Marshall (2), it can be assumed that the increase in width is virtually limited to the entrance zone up to where the peak pressure is obtained. The actual flow in the nip area is further complicated because the gap clearance varies axially as a result of built-in roll-crowns, hydrodynamic flexing, and bending of the rolls. All these factors should bring about a flow distribution in the nip area that results in

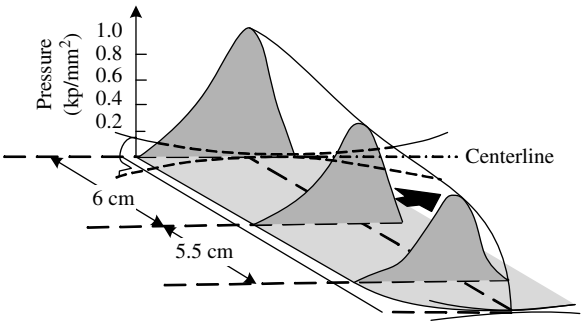

Fig. 15.3 Pressure profiles in the calender gap at various cylinder axial positions, with rigid PVC (Vestolit Z 1877) at equal roll speeds of 5 cm/s and roll temperature of 185°C: minimum gap, 0.6 mm; roll diameter, 30 cm; width, 50 cm. Note the drop in pressure in the cross-machine direction with distance from the centerline, which drops to zero at the end of the rolled web. [Reprinted by permission from W. Unkrüer, Doctoral Thesis, IKV, Technischen Hochschule, Aachen, 1970.]

uniform flow rate per unit width. Minor variations of pressure profiles in the direction of rotation will cause variations in detachment locations, and hence, thickness variations.

In light of the preceding qualitative picture, we can understand recent developments in a modified calendering process, where an extruder equipped with a simple and short sheet forming die feeds the nips uniformly throughout the nip width of only one pair of calender rolls. The sheet forming die therefore performs the functions of the first nip—namely, spreading out the material and feeding it at a more or less uniform rate to the second nip.

The functions of the second and third nips are a further reduction of the thickness and of the flow rate nonuniformities in both the machine and cross-machine directions. The rolling banks in all nips act as reservoirs that can accommodate and attenuate flow rate fluctuations. Thus, no sharp qualitative distinction should be made between the functions of the three nips; it is the relative significance of the various functions that changes from nip to nip. All nips ''meter'' flow rate, reduce thickness, and ''wash out'' variations in thickness and flow rate to various degrees (just as in plasticating screw extruders, flow rate is determined by the whole length of the screw, not merely by the ''metering'' section). Clearly there is no simple analytical mathematical solution to this three-dimensional flow in a complex geometry (variable gap thickness in two directions) with rheologically complex fluids under nonisothermal conditions.

Most models proposed in the literature are based on Gaskell's (4) model, which was discussed in detail in Section 6.4. This is a one-dimensional, rather restrictive model. Recall that to use the model, we must know the location X_1 where the sheet detaches from one of the rolls (X_1 is uniquely related to X_2, the upstream location where the rolls come in contact with the polymer). This is tantamount to an a priori knowledge of the exiting sheet thickness, $2H_1$. The latter, however, for a given flow rate, Q, depends on the exiting sheet width W_1

$$Q = 2H_1 W_1 U \tag{15.2-1}$$

where U is the velocity of the roll surface. But W_1 cannot be predicted from a one-dimensional model (which implicitly assumes infinitely wide rolls), hence as McKelvey (5) pointed out, X_1 (or H_1) must be considered to be an experimentally determined parameter of the model. This, of course, restricts the predictive capability of the model. To overcome this problem, the previously discussed cross-machine flow must be incorporated into the model.

This, however, is not the only limitation of the Gaskell model. As discussed in Section 6.4, this model fails to predict the experimentally observed flow patterns in the inlet region because it neglects the effect of the incoming melt stream on the flow in the bank, as well as the non-Newtonian and viscoelastic effects. Consequently, the model does not satisfactorily predict the observed pressure profiles, as shown by Bergen and Scott (6), Unkrüer (3), and others.

Following Gaskell's work, a great deal of effort was invested by numerous researchers in the field to improve on his model. Most of this effort, however, basically concentrated on solving the Gaskell model with more realistic, constitutive equations and attempts to account for nonisothermal effects. In the original Gaskell model, a purely viscous (nonelastic and time-independent) fluid model is assumed, with specific

solutions for Newtonian and Bingham Plastic fluids, and a brief treatment of nonsymmetric calenders. McKelvey (5) and Brazinsky et al. (7) extended the model to Power Law fluids (as discussed in Section 6.4), and Alston and Astill (8) investigated fluids whose shear rate dependent viscosity can be represented by a hyperbolic tangent function.

Flow of viscoelastic fluids in the roll geometry was considered by Paslay (9) and Tokita and White (10), and by Chong (11); Paslay's analysis is essentially based on a three constant Oldroyd model.[1] He analyzes the interrelations of the parameters of the constitutive equation with flow kinematics, but neglects the normal stresses in the equation of motion. Tokita and White (10) relate experimental observations on milling of elastomers to rheological parameters of a second order Rivlin–Ericksen asymptotic expansion fluid, and point out the significance of the Deborah number $\mathrm{De} = \dot{\gamma}\lambda \cong (V/L)\lambda$ in milling and calendaring, where V and L are characteristic velocity and gap size. Following their analysis, Example 15.1 briefly explores the significance of normal stresses in calendering. However velocity and pressure profiles were not obtained by them.

Chong (11) analyzed a Power Law model fluid, a three-constant Oldroyd fluid and a modified second order Rivlin–Ericksen fluid. He incorrectly stated that the shear rate and the shear stress attain maximum values at minimum clearance location, and in integrating for the velocity profile with the Power Law model fluids, did not properly account for the sign of the pressure gradient. The velocity profile for the Oldroyd fluid cannot be obtained analytically. Therefore Chong obtained an approximate pressure distribution by assuming Newtonian flow kinematics, and he analyzed the flow pattern with the Rivlin–Ericksen flow equation in terms of dimensionless groups only. He also measured the separating force at various calendering conditions for cellulose acetate. Like Tokita and White (10), he found, upon analyzing experimental data of calendering cellulose acetate, that the Deborah number is an important number in determining the onset of a nonuniform internal strain pattern, called *nerve* in calendering. Calendering defects with PVC were studied in detail by Agassant et al. (12), who also measured separating force, torque power, and reservoir height-to-gap ratio (H_2/H_0) as a function of calendering conditions.

With regard to constitutive equations, White (13) notes that, in view of the short residence time of the polymer in the nip region (of the order of magnitude of seconds), it would be far more realistic to use a constitutive equation that includes viscoelastic transient effects such as stress overshoot, a situation comparable to that of squeezing flows discussed in Section 6.6.

Example 15.1 The Significance of Normal Stresses We consider the calender geometry of Fig. 6.22 (shown here) and make the same simplifying assumptions as in Section 6.4, but instead of a Newtonian or Power Law model fluid, we assume a CEF model that exhibits normal stresses in viscometric flows. By accepting the lubrication approximation, we assume that locally we have a fully developed viscometric flow because there is only one velocity component v_x, which is a function of only one spatial variable y.

1. The three constant Oldroyd model is a nonlinear constitutive equation of the differential corrotational type, such as the Zaremba–Fromm–Dewitt (ZFD) fluid (Eq. 3.3-11). [For details, see R. B. Bird, R. C. Armstrong, and O. Hassager, *Dynamics of Polymeric Liquids*, Second Edition, Vol. 1, Wiley, New York, 1987, Table 7.3-2.]

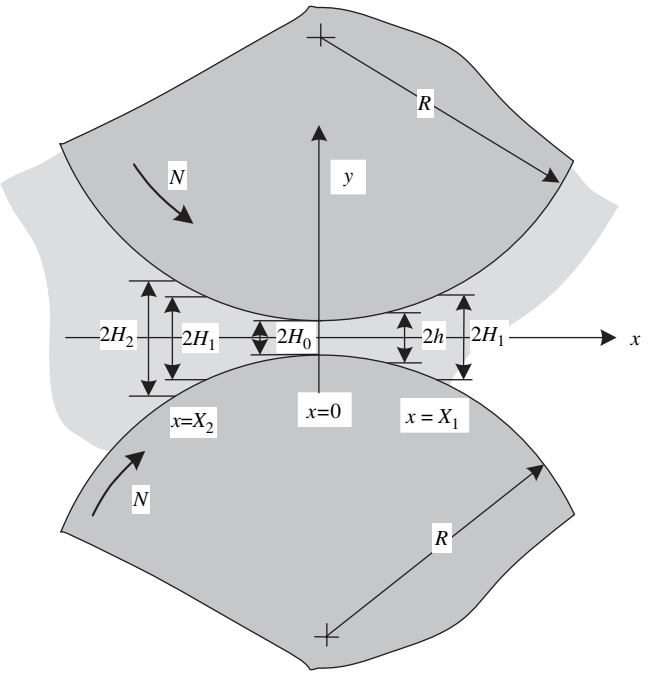

An analysis similar to that carried out in Section 6.5 leads to the following, nonvanishing stress components

$$\tau_{xx} = -(\Psi_1 + \Psi_2)\dot{\gamma}^2 \tag{E15.1-1}$$

$$\tau_{yy} = -\Psi_2\dot{\gamma}^2 \tag{E15.1-2}$$

where $\dot{\gamma} = |\dot{\gamma}_{yx}|$ is the shear rate and

$$\dot{\gamma}_{yx} = \frac{dv_x}{dy} \tag{E15.1-3}$$

which is assumed to be independent of x locally. The three components of the equation of motion then reduce to

$$\frac{\partial P}{\partial x} = -\frac{\partial \tau_{yx}}{\partial y} \tag{E15.1-4}$$

$$\frac{\partial P}{\partial y} = -\frac{\partial \tau_{yy}}{\partial y} \tag{E15.1-5}$$

$$\frac{\partial P}{\partial z} = 0 \tag{E15.1-6}$$

Comparing with the solution in Section 6.4, we observe that instead of a single differential equation for the velocity profile, two coupled (through $\dot{\gamma}$) differential equations are obtained. However, the kinematics can be well approximated by assuming $\partial P/\partial y = 0$, which then will

lead to the same velocity profile given in Section 6.4. Moreover, we note that the pressure at the roll surface will differ from that of the simple model by a term $-\Psi_2\dot{\gamma}^2$. Since Ψ_2 is found to be negative, this normal stress contribution adds to the pressure at the roll surface. Hence, it is the secondary normal difference function that plays a role in calculating the forces on the calender roll. This can probably be assumed to be small.

The present analysis was based on the lubrication approximation; that is, we neglected changes in the x direction. If this assumption is lifted, we are faced with a flow field in which two nonvanishing velocities exist that are functions of two spatial coordinates, $v_x(x, y)$, $v_y(x, y)$. This is clearly a nonviscometric flow situation, and the Criminale–Ericksen–Filbey (CEF) equation is not applicable. White (13) made an order of magnitude evaluation of normal stress effects for this more realistic flow situation. In this case, the equation of motion reduces to

$$-\frac{\partial P}{\partial x} = \frac{\partial \tau_{yx}}{\partial y} + \frac{\partial \tau_{xx}}{\partial x} \tag{E15.1-7}$$

and

$$-\frac{\partial P}{\partial y} = \frac{\partial \tau_{yx}}{\partial x} + \frac{\partial \tau_{yy}}{\partial y} \tag{E15.1-8}$$

which can be combined by respective differentiation into one equation

$$\frac{\partial^2 \tau_{yx}}{\partial y^2} - \frac{\partial^2 \tau_{yx}}{\partial x^2} + \frac{\partial^2}{\partial x \partial y}\left(\tau_{xx} - \tau_{yy}\right) = 0 \tag{E15.1-9}$$

Expressing the various terms in Eq. E15.1-9 at the roll surface as orders of magnitude, we get

$$\frac{\tau_w}{H_0^2}; \qquad \frac{\tau_w}{R^2}; \qquad \frac{\tau_{xx} - \tau_{yy}}{H_0 R} \tag{E15.1-10}$$

where H_0 and R are gap clearance and roll radius, respectively. If $R \gg H_0$, the second term is negligible. The third term, which reflects the primary normal stress difference, is also negligible, provided

$$\frac{R}{H_0}\tau_w \gg \tau_{xx} - \tau_{yy} \tag{E15.1-11}$$

The preceding condition is met at low shear rates, but it begins to break down with increasing shear rate when $\tau_{xx} - \tau_{yy}$ increases rapidly, as indicated in Fig. E3.2b.

In the Gaskell model, the flow geometry is simplified to facilitate the solution (see Eq. 6.4-13). This geometrical simplification can be avoided either by using bipolar coordinates or finite element methods (FEMs). Both provide a convenient way to treat calenders of unequal rolls and unequal speeds. The former approach was taken by Finston (14), Takserman-Krozer et al. (15), and Bekin et al. (16), whereas the latter was chosen by Kiparissides and Vlachopoulos (17). Finally, the Gaskell model is isothermal, whereas in calendaring, significant nonisothermal effects arise because of viscous dissipation and heat conduction to the temperature-controlled rolls.

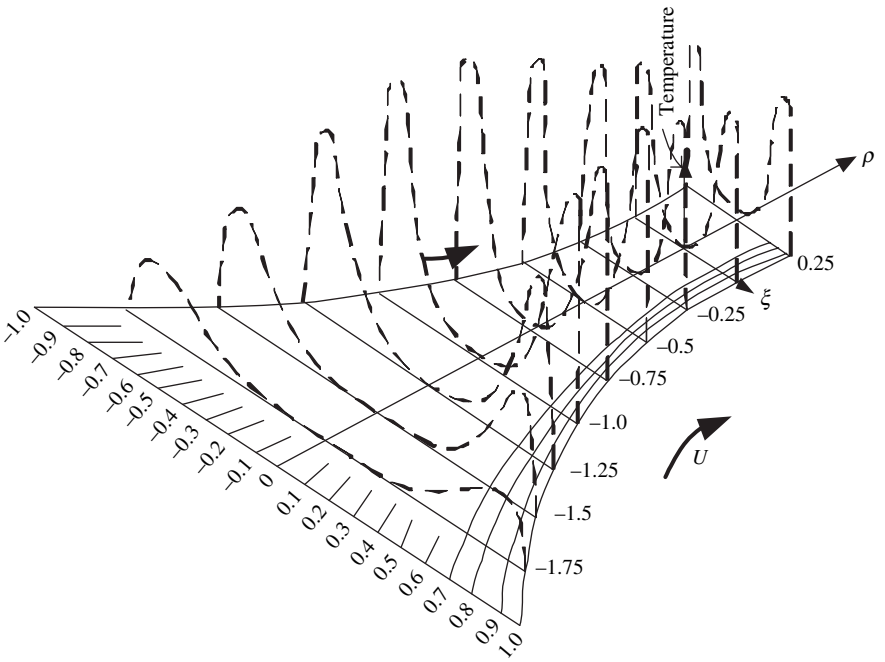

Fig. 15.4 Schematic temperature distribution based on data given by Torner (18).

Finston (14) was the first to deal with viscous heating of Newtonian fluids. Torner (18) reported on an experimental study by Petrusanskii and Stachaev (19) on the calendering of styrene-butadiene rubber (SBR) on a 12 × 32-cm calender. Figure 15.4 is a schematic view of the reported temperature profiles. Characteristic to the temperature profiles is the existence of two maxima in the vicinity of the rolls. This is the combined effect of a shear rate profile with a maximum value at the roll surface and heat conduction to the temperature-controlled roll surface. The temperature profile has a minimum at the center plane. The temperature profiles change in the machine direction, with a gradual temperature rise at the center plane and more complex behavior in the vicinity of the rolls. It should be noted that these temperature profiles do not refer to recirculating regions in the entry to the calender gap. Temperature effects were also studied by Bekin et al. (16), using bipolar coordinates and temperature dependent fluid viscosity.

15.3 ANALYSIS OF CALENDERING USING FEM

The FEM, which was originally developed for structural analysis of solids, has been very successfully applied in the past decades to viscous fluid flow as well. In fact, with the exponentially growing computer power, it has become a practical and indispensable tool for solving complex viscous and viscoelastic flows in polymer processing (20) and it is the core of the quickly developing discipline of computational fluid mechanics (cf. Section 7.5).

One of the first applications of FEM in polymer processing is a result of the work of Vlachopoulos and Kiparissides (21,22). Some of the computed results obtained by this

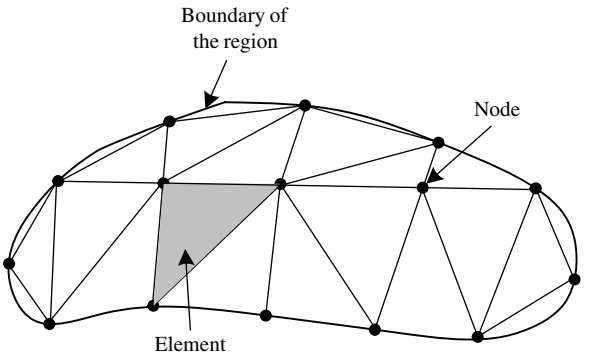

Fig. 15.5 Two-dimensional region represented as an assemblage of triangular elements.

method are discussed later in this chapter. The use of FEM in calendering has the added advantage that it can, in principle, be combined with a structural FEM analysis of the rolls accounting for roll deflections.

The principles and applications of FEM are described extensively in the literature (e.g., 23–26). FEM is a numerical approximation to continuum problems that provides an *approximate*, piecewise, continuous representation of the unknown field variables (e.g., pressures, velocities).

The continuous region or body is subdivided into a *finite* number of subregions or *elements* (Fig. 15.5). The elements may be of variable size and shape, and they are so chosen because they closely fit the body. This is in sharp contrast to finite difference methods, which are characterized by a regular size mesh, describable by the coordinates that describe the boundaries of the body.

The crossing of two curves bounding adjacent elements form *nodes.* The values of the field variables at the nodes form the desired solution. Common shapes of finite elements are triangular, rectangular, and quadrilateral in two-dimensional problems, and rectangular, prismatic, and tetrahedral in three-dimensional problems. Within each element, an interpolation function for the variable is *assumed.* These assumed functions, called *trial functions* or *field variable models*, are relatively simple functions such as truncated polynomials. The number of terms (coefficients) in the polynomial selected to represent the unknown function must at least equal the degrees of freedom associated with the element. For example, in a simple one-dimensional case [Fig. 15.6(a)], we have two degrees of freedom, P_i and P_j, for a field variable $P(x)$ in element e. Additional conditions are needed for more terms (e.g., derivatives at nodes i and j or additional internal nodes).

The chosen function must satisfy certain additional requirements. Not only must it be continuous throughout the element, but also compatible across element interfaces. In the simple case [Fig. 15.6(b)], this means $P_a = P_b$ at the node m is common to elements a and b. Thus the coefficients of a selected trial function can be expressed in terms of the (unknown) values of the field variables at the nodes. For a two-dimensional case we can write for the field variable u,

$$u^{(m)}(x, y) = \sum_{i=1}^{r} N_i(x, y) u_i^{(m)} \tag{15.3-1}$$

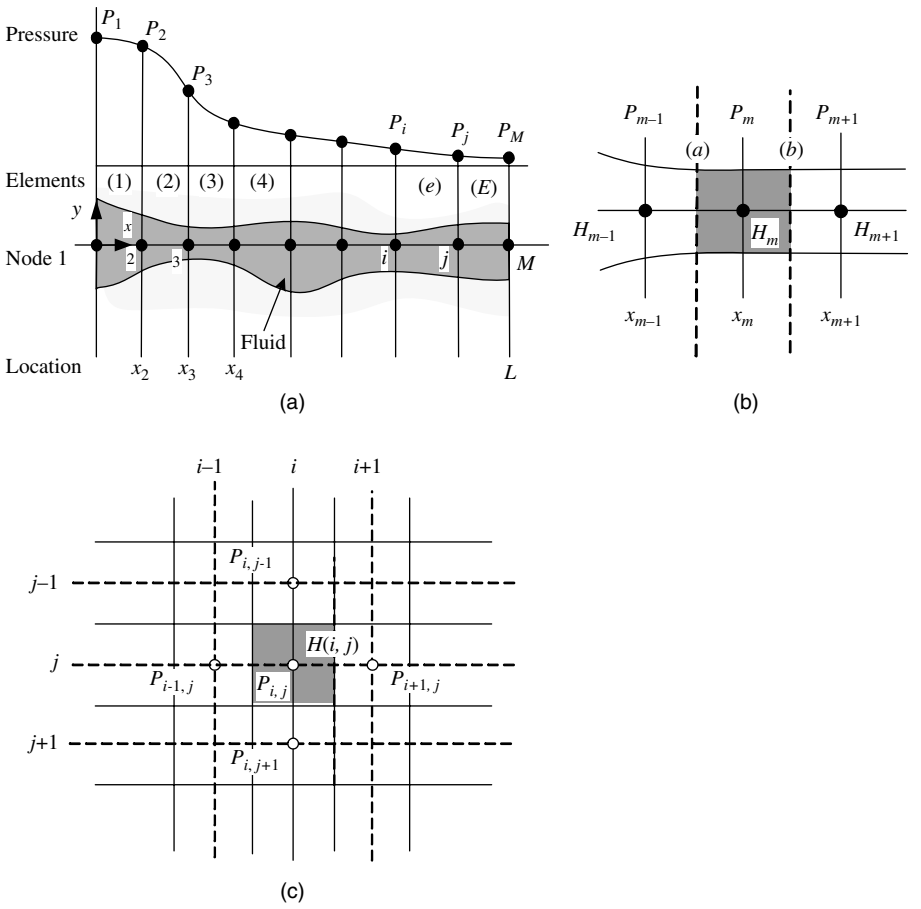

Fig. 15.6 (a) Side view of two infinite plates with a variable gap in the x direction. The region of interest $0 < x < L$ is broken up into E elements forming M nodes. A schematic pressure profile for one-dimensional pressure flow is plotted on the top. (b) Details of two neighboring elements a and b with the common node m. (c) Two-dimensional square elements representing flow analysis network model.

where the superscript denotes that the field is for the mth element, r is the number of nodes associated with this element, $u_i^{(m)}$ are the nodal values of the variable u, and $N_i(x,y)$ is the *shape function.* The function $N_i(x,y)$ is determined by the shape of the element, the location of the nodes, and the number of terms in the polynomial. Again, the objective is the numerical evaluation of u_i. The common approach to obtaining this is to set up the finite element equations either by ''variational'' methods or by ''residual'' methods, such as the *Galerkin method.* These, together with appropriate boundary conditions, result in a set of linear or nonlinear algebraic equations with the nodal variables u_i as unknowns.

Structural analysis, initially developed on an intuitive basis, later became identified with variational calculus, in which the Ritz procedure is used to minimize a *functional* derived mathematically or arrived at directly from physical principles. By substituting the final solutions into the variational statement of the problem and minimizing the latter, the FEM equations are obtained. Example 15.2 gives a very simple demonstration of this procedure.

However, in many cases (general non-Newtonian flow problems being among them), a variational principle either does not exist or its existence is not obvious. Nevertheless, these problems can often be defined by a set of differential equations (e.g., the equations of continuity and motion with a constitutive equation), together with their boundary conditions. In such cases, weighted residual methods such as the collocation and the Galerkin methods produce a simpler and direct formulation of the FEM equations (27). In the Galerkin method, the approximate interpolation function is substituted into the governing differential equations, multiplied by the weighting function, which is the relevant shape function, and integrated over the body. The resulting expressions are set to zero, leading to a set of algebraic equations.

Inherent in the FEM is the flexibility in dealing with complex geometries as well as mixed boundary conditions (e.g., stress and velocity boundary conditions as in a die-swell problem). Moreover, computationally, the FEM is not difficult to carry out. Not only can a continuous domain of complex boundary be easily broken down into well-fitting finite elements, but the inherent possibility exists of using elements of various sizes and shapes. This permits a refined solution in critical regions (corners, sudden changes in geometry, etc.) without the penalty of excessive computation in the rest of the regions, as would be the case with the more limited finite difference methods. Finally, it is noted by Oden et al. (28) that by certain function choices, the standard finite difference processes can be included in the general finite-elements concept.

Example 15.2 FEM Formulation of Isothermal Steady Pressure Flow in Narrow but Variable Thickness Gap of a Newtonian Fluid The governing differential equation is the Reynolds equation given for a two-dimensional flow in Eq. 2.11-11. To demonstrate the FEM formulation, we consider the one-dimensional flow case, for which Eq. 2.11-11 reduces to

$$\frac{d}{dx}\left(\frac{H(x)^3}{\mu}\frac{dP}{dx}\right) = 0 \tag{E15.2-1}$$

We have retained the viscosity because we want to treat approximately the non-Newtonian fluids case later. If the function $H(x)$ is known, preceding the differential equation can be solved analytically or numerically for $P(x)$ in a straightforward method without turning to FEM. Our purpose here, however, is to demonstrate the FEM method and, following Myers (29), we do so in a step-by-step fashion.

The flow configuration appears in Fig. 15.6(a). The one-dimensional conduit of length L is broken down into E elements, bounded by M nodes. Our objective is to set up the FEM equations that will give the pressure values P_i.

The first step is to derive the *variational statement* of the problem. This can be done with the aid of the Lagrange–Euler equation

$$\frac{\partial F}{\partial P} - \frac{d}{dx}\left(\frac{\partial F}{\partial \dot{\boldsymbol{P}}}\right) = 0 \tag{E15.2-2}$$

which must be satisfied for the following *functional* I

$$I = \int_0^L F(x, P, \dot{\boldsymbol{P}})\, dx \tag{E15.2-3}$$

to be an *extremum.* Comparison of Eqs. E15.2-1 and E15.2-2 gives the following expressions for *F:*

$$\frac{\partial F}{\partial P} = 0 \tag{E15.2-4}$$

and

$$\frac{\partial F}{\partial \dot{P}} = \frac{H^3}{\mu}\dot{P} \tag{E15.2-5}$$

Integration of Eqs. E15.2-4 and E15.2-5, respectively, gives

$$F = K_0 + f(\dot{P}) \tag{E15.2-6}$$

and

$$F = \frac{H^3}{2\mu}(\dot{P})^2 + g(P) \tag{E15.2-7}$$

Comparing Eqs. E15.2-6 and E15.2-7, we note $g(P) = K_0$ and $f(\dot{P}) = (H^3/2\mu)(\dot{P})^2$; thus, F can be written as

$$F = K_0 + \frac{1}{2}\frac{H^3}{\mu}(\dot{P})^2 \tag{E15.2-8}$$

Hence, the variational statement of this problem reduces to obtaining the extremum of the functional

$$I = \int_0^L \left[K_0 + \frac{1}{2}\frac{H^3}{\mu}(\dot{P})^2\right] dx \tag{E15.2-9}$$

that is, we are searching for the unknown *function* $P(x)$ that, when substituted into Eq. E15.2-9, gives an extremum for I. To evaluate I, we break it down into E subintegrals corresponding to the E elements

$$I = I^{(1)} + I^{(2)} + \cdots + I^{(E)} = \sum_{e=1}^{E} I(e) \tag{E15.2-10}$$

The integral $I^{(e)}$ over a typical finite element is

$$I^{(e)} = \int_{x_i}^{x_i} \left[K_0 + \frac{1}{2}\frac{H^3}{\mu}(\dot{P})^2\right] dx \tag{E15.2-11}$$

We now *assume* a linear trial function for the variation of the pressure within each element

$$P^{(e)} = C_1^{(e)} + C_2^{(e)} x \tag{E15.2-12}$$

We thus have two coefficients, and since we have two degrees of freedom—the (unknown) nodal values of the pressures—we can express the former in terms of the latter, and Eq. E15.2-12 can be written as

$$P^{(e)} = \left(\frac{x_j - x}{x_j - x_i}\right)P_i + \left(\frac{x - x_i}{x_j - x_i}\right)P_j \tag{E15.2-13}$$

Note that Eq. E15.2-13 is of the same form as Eq. 15.3-1. Next we take the derivative of $P^{(e)}$ given in Eq. E15.2-13 with respect to x

$$\dot{P} = \frac{dP^{(e)}}{dx} = \frac{P_j - P_i}{x_j - x_i} \tag{E15.2-14}$$

and substitute it into Eq. E15.2-11 which, after integration, gives

$$I^{(e)} = K_0(x_j - x_i) + \frac{1}{2}\frac{H^3}{\mu}\frac{(P_j - P_i)^2}{(x_j - x_i)} \tag{E15.2-15}$$

We have assumed in the foregoing integration that μ is constant within the element and equal to the average value in it.

Next we differentiate $I^{(e)}$ with respect to the nodal pressures P_i and P_j

$$\frac{\partial I^{(e)}}{\partial P_i} = -\frac{H^3}{\mu}\frac{P_j - P_i}{x_j - x_i} \tag{E15.2-16}$$

and

$$\frac{\partial I^{(e)}}{\partial P_j} = \frac{H^3}{\mu}\frac{P_j - P_i}{x_j - x_i} \tag{E15.2-17}$$

where $I^{(e)}$ is a function of P_i and P_j only, whereas I (in Eq. E15.2-10) is a function of P_1, $P_2, \ldots, P_M$. To find the extremum of I, we must differentiate I with respect to all P_i, and set the results equal to zero, obtaining M equations. Thus, differentiating Eq. E15.2-10 with respect to a typical nodal pressure P_m, we get

$$\frac{\partial I}{\partial P_m} = \frac{\partial I^{(1)}}{\partial P_m} + \frac{\partial I^{(2)}}{\partial P_m} + \cdots + \frac{\partial I^{(E)}}{\partial P_m} = 0 \tag{E15.2-18}$$

But the pressure P_m appears only in two neighboring elements, as Fig. 15.6(b) shows. For element a we set $i = m - 1$ and $j = m$ in Eqs. E15.2-16 and E15.2-17, and for element b we set $i = m$ and $j = m + 1$ in the two previous equations, resulting in

$$\frac{\partial I^{(a)}}{\partial P_m} = \left(\frac{H^3}{\mu}\right)^{(a)}\frac{P_m - P_{m-1}}{x_m - x_{m-1}} \tag{E15.2-19}$$

and

$$\frac{\partial I^{(b)}}{\partial P_m} = -\left(\frac{H^3}{\mu}\right)^{(b)} \frac{P_{m+1} - P_m}{x_{m+1} - x_m} \tag{E15.2-20}$$

where the superscripts a and b on H^3/μ indicate that mean local values are used. Adding Eqs.E15.2-19 and E15.2-20, and equating the sum to zero, we get

$$\left(\frac{H^3}{\mu}\right)^{(a)} \frac{P_m - P_{m-1}}{x_m - x_{m-1}} + \left(\frac{H^3}{\mu}\right)^{(b)} \frac{P_m - P_{m+1}}{x_{m+1} - x_m} = 0 \tag{E15.2-21}$$

Since m is any interior nodal point, Eq. E15.2-21 is a set of $M - 2$ algebraic equations, the solution of which provides the required pressure field (profile).

As a numerical example, consider a linearly decreasing gap broken down into four equal length elements. The gaps at the entrance and at the exit are 1 and 0.5 cm, respectively. Thus $H_1 = 1$, $H_2 = 0.875$, $H_3 = 0.75$, $H_4 = 0.625$, and $H_5 = 0.5$. The inlet pressure is 1 atm, and the exit pressure is zero. The resulting equations from Eq. E15.2-21, with constant viscosity, are

$$\begin{aligned} -1.53618 + 2.53618P_2 - P_3 &= 0 \\ -1.6506P_2 + 2.6506P_3 - P_4 &= 0 \\ -1.8257P_3 + 2.8257P_4 &= 0 \end{aligned}$$

which, upon solution, give $P_2 = 0.897$, $P_3 = 0.738$, and $P_4 = 0.477$. The exact analytical solutions obtained by integrating Eq. E15.2-1 are $P_2 = 0.8980$, $P_3 = 0.7407$, and $P_4 = 0.480$, which agree well with the FEM solution using only four elements.

Equation E15.2-21 can also be derived by a ''controlled volume'' approach. Consider the a element confining node m in Fig. 15.6(b) (shaded area). For an incompressible fluid and under the same assumptions as earlier we can make the following flow rate balance

$$\underbrace{\frac{1}{12}\left(\frac{H^3}{\mu}\right)^{(a)} \frac{P_{m-1} - P_m}{x_m - x_{m-1}}}_{\substack{\text{Rate of flow} \\ \text{into element}}} = \underbrace{\frac{1}{12}\left(\frac{H^3}{\mu}\right)^{(b)} \frac{P_m - P_{m+1}}{x_{m+1} - x_m}}_{\substack{\text{Rate of flow} \\ \text{out of element}}} \tag{E15.2-22}$$

The FEM formulation of two-dimensional problems is not different in principle from the simple one-dimensional case just described. For two-dimensional problems, however, the algebra becomes involved and matrix notation is required to keep it manageable.

Example 15.3 The Flow Analysis Network Method Clearly Eq. E15.2-22 is identical to Eq. E15.2-21. This is the basis for the flow analysis network (FAN) method developed by Tadmor et al. (30) to solve two-dimensional steady or quasi-steady state flow problems in injection molds and extrusion dies. In two-dimensional flows the pressure distribution is obtained by dividing the flow region into an equal-sized mesh of square elements

[Fig. 15.6(c)]. At the center of each element there is a node. The nodes of adjacent elements are interconnected by links. Thus, the total flow field is represented by a network of nodes and links. The fluid flows out of each node through the links and into the adjacent nodes of the network. The local gap separation determines the ''resistance'' to flow between nodes. Making the quasi–steady state approximation, a mass (or volume) flow rate balance can be made about each node (as done earlier for one-dimensional flow), to give the following set of algebraic equations

$$X_{i,j}(P_{i,j} - P_{i+1,j}) + X_{i-1,j}(P_{i,j} - P_{i-1,j}) + Z_{i,j}(P_{i,j} - P_{i,j+1}) + Z_{i,j-1}(P_{i,j} - P_{i,j-1}) = 0 \tag{E15.3-1}$$

where $X_{i,j}$ and $Z_{i,j}$ are ''flow conductances'' in the x and z directions, respectively:

$$X_{i,j} = \frac{1}{12\mu}\left(\frac{H_{i,j} + H_{i+1,j}}{2}\right)^3 \tag{E15.3-2}$$

and

$$Z_{i,j} = \frac{1}{12\mu}\left(\frac{H_{i,j} + H_{i,j+1}}{2}\right)^3 \tag{E15.3-3}$$

This two-dimensional formulation of the flow problem is identical in concept to the ''discrete element method'' or ''lattice models'' of classic structural analysis. Physically, the FEM concept differs from the lattice analogy in that the elements themselves are two- or three-dimensional bodies (31). The FAN method, however, is a straightforward, simple method, which was extended to deal with non-Newtonian fluids by replacing the Newtonian viscosity with an ''equivalent Newtonian viscosity'' (32). The latter is uniquely related to the local shear stress at the wall, which in turn depends on the local pressure gradient. Both can be converged upon by repeated solutions of the set of algebraic equations for P_{ij}, while in each iteration, the viscosities are recalculated. This method was applied by Tadmor et al. to cross-head die flow (33), mold filling (34), and flow in non-intermeshing twin screw extruders (35). White et al. (36) extended the method and applied it to intermeshing corrotating twin screw extrusion flow. Both are two-dimensional, the first being steady while the second is assumed to be quasi–steady.

Mitsoulis, Vlachopoulos, and Mirza (37) were the first to lift the lubrication approximation in calendering flows and use FEM computational packages to obtain the flow and temperature fields in the bank and nip regions, with which we can calculate the pressure distribution, roll-separating force, torques, and power consumption to drive the rolls, as well as the nip entry and exit locations and the exit sheet thickness. They did the analysis for a Newtonian and a Power Law model fluid, with rheological constants representing a rigid PVC melt, which also exhibits slip (38). The FEM results are in fair agreement with experiments, but give only axysymmetric circulatory flows in the melt pool upstream from the nip. Park et al. (39) used the viscoelastic integral type Kaye-Bernstein- Kearsky-Zappas (K-BKZ) fluid model to simulate the converging flow using an FEM. Luo (40) used a finite volume method (FVM) and the integral K-BKZ to calculate the converging flow. Both groups of investigators did not integrate their fluid-mechanical results with the resulting roll deformations.

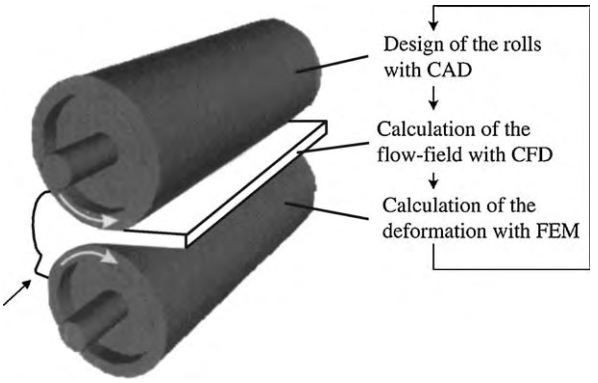

Fig. 15.7 Iterative computational scheme used by Mewes et al. [Reprinted by permission from D. Mewes, S. Luther, and K. Riest, "Simultaneous Calculation of Roll Deformation and Polymer Flow in the Calendering Process," *Int. Polym. Process.*, **17**, 339–346 (2002).]

Recently, Mewes (41) utilized the FVM CFX4 computational package of Luo (40) and integrated it with the ANSYS solids structural FEM model to calculate the resulting roll deformations. The rolls were designed using a computer-aided design (CAD) program. Their iterative computational scheme is shown in Fig. 15.7.

The calender roll diameter profiles are designed using the CAD Pro/Engineer program and the isothermal flow field is calculated using the computational fluid mechanics FVM. With the resulting stress field as boundary conditions, the deformation of the rolls is calculated using ANSYS. If the resulting gap thickness determined by the initial diameter axial profile, flow, and axial separation force profile do not yield a uniform gap thickness, then the CAD design is changed as many times as it takes to obtain a gap spacing for the calendered material thickness that is uniform, that is, independent of the axial roll distance.

Conducting iterative flow calculations per se for given initial roll design was not carried out, since this requires large computational times. Three constitutive equations were used by Mewes et al: the K-BKZ with a damping function formulation by Papanastasiou et al. (42) for the polymer melt [a low density polyethylene (LDPE)]; a three-dimensional Hooke's law for multiaxial strains (43) and the relation between the Poison ratio (v), shear (G), and tensile (E) moduli $G = E/2(1 + v)$ for the steel; and a Mooney–Rivlin hyperelastic model (44) for the cross-linked elastomer lining of one of the rolls. All the rheological parameters have to be evaluated. Details of the constitutive equations, parameters, and the computational details are given in the paper by Mewes et al. (41).

Computed values of the primary normal stress difference of a low molecular weight polyisobutelene (PIB) melt we compared with experimentally obtained values, using bire fringence techniques, as shown on Fig. 15.8; they indicate good agreement.

The effect of changing the longest relaxation time of the K-BKZ and the primary normal stress difference is shown in Fig. 15.9.

Fig. 15.10(a) represents schematically the roll deformation along the roll axes, z, caused by the flow of a K-BKZ fluid. Figure 15.10(b) plots the initial roll-diameter profile

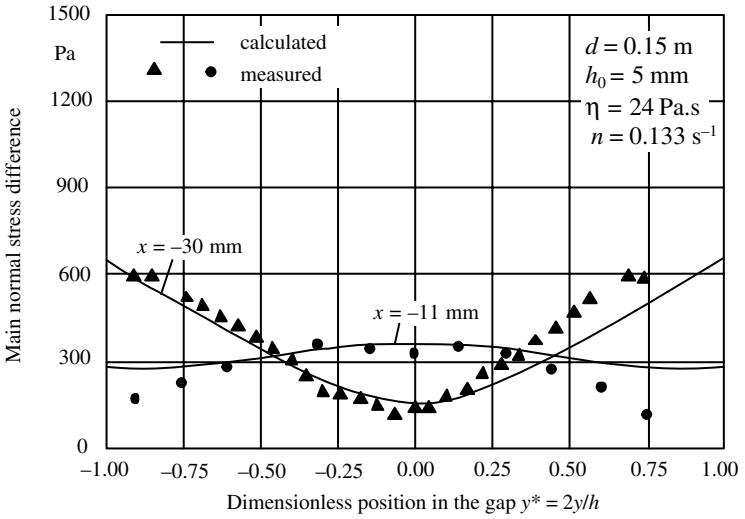

Fig. 15.8 Calculated and measured differences of the primary normal stresses in the calender gap for two different planes; $y_{(x=0)} = H_0/2$. [Reprinted by permission from D. Mewes, S. Luther, and K. Riest, ''Simultaneous Calculation of Roll Deformation and Polymer Flow in the Calendering Process,'' *Int. Polym. Process.*, **17**, 339–346 (2002).]

(''tangential deviation''), the roll deformation due to flow, and the resulting, almost constant gap thickness. The desired constant gap thickness is due to the compensating deformation and initial rolls profiles, as seen in the figure. Finally, for a pair of rolls, one of which is ''rigid'' steel and the other coated with a deformable, hyperelastic fluid elastomer,

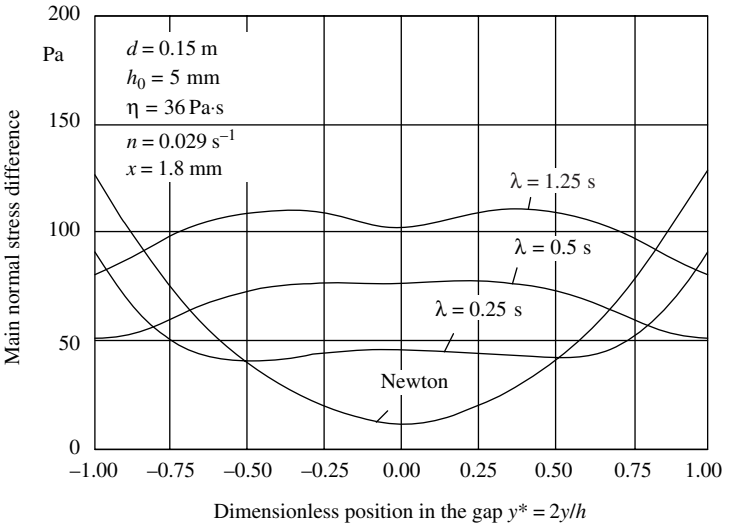

Fig. 15.9 Primary normal stress differences in the calender gap calculated with the K-BKZ model for different relaxation times. [Reprinted by permission from D. Mewes, S. Luther, and K. Riest, ''Simultaneous Calculation of Roll Deformation and Polymer Flow in the Calendering Process,'' *Int. Polym. Process.*, **17**, 339–346 (2002).]

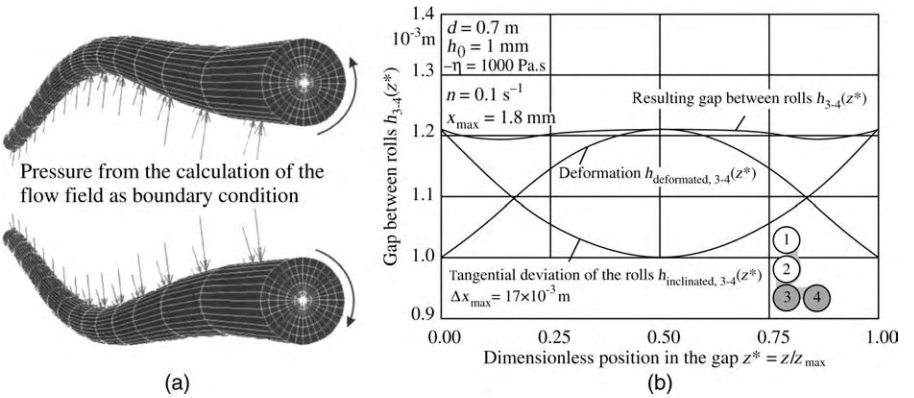

Fig. 15.10 (a) Representation of the deformation between rolls 3 and 4 of a calender design used by Mewes at al. (41); not to scale (b) calculated gap uniformity, resulting from the initially imposed roll diameter and the roll deformation for rolls 3 and 4. [Reprinted by permission from D. Mewes, S. Luther, and K. Riest, "Simultaneous Calculation of Roll Deformation and Polymer Flow in the Calendering Process," *Int. Polym. Process.*, **17**, 339–346 (2002).]

the flow stresses in the nip deform the elastomer coats. Figure 15.11 depicts the calculated von Mises stresses

$$\sigma_{\text{Mises}} = \sqrt{\frac{1}{2}\left[(\sigma_1 - \sigma_2)^2 + (\sigma_2 - \sigma_3)^2 + (\sigma_3 - \sigma_1)^2\right]}$$

in the elastomeric coat and the flow pressure buildup, both in the circumferential direction.

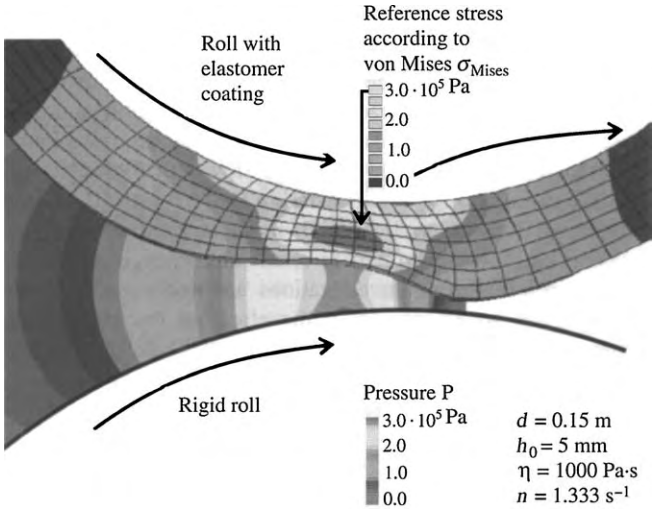

Fig. 15.11 Representation of the pressure in the flow field and the deformation of the elastomer coating. [Reprinted by permission from D. Mewes, S. Luther, and K. Riest, "Simultaneous Calculation of Roll Deformation and Polymer Flow in the Calendering Process," *Int. Polym. Process.*, **17**, 339–346 (2002).]

The ANSYS program is used to calculate the deformations and stresses in the elastomeric coat.

The preceding work demonstrates the benefits of combining CAD design, computational fluid mechanics (in this case a FVM CFX4), and a solids deformation ANSYS program to solve the ''complete'' calendering program and, thus, arrive at a computer roll design that points to a promising uniform sheet production for a given polymer melt and operating conditions. Of course, more realistic solutions, such as the simulation of the nonisothermal flow and roll temperature case, are obtainable with sufficient computing power.

REFERENCES

1. G. W. Eighmy, Jr., ''Calendering,'' in *Modem Plastics Encyclopedia*, McGraw-Hill, New York, 1977, p. 234.
2. D. I. Marshall, ''Calendering,'' in *Processing of Thermoplastics Materials*, E. C. Bernhardt, Ed., Reinhold, New York, 1959, Chapter 6.
3. W. Unkrüer, ''Beitrag zur Ermittlung des Druckverlaufes und der Fliessvorgange im Walzsplat bei der Kalanderverarbeitung von PVC Hart zu Folien,'' Doctoral Thesis, IKV, Technischen Hochschule, Aachen, Germany, 1970.
4. R. E. Gaskell, ''The Calendering of Plastic Materials,'' *J. Appl. Mech.*, **17**, 334–336 (1950).
5. J. M. McKelvey, *Polymer Processing*, Wiley, New York, 1962, Chapter 9.
6. J. T. Bergen and G. W. Scott, ''Pressure Distribution in Calendering of Plastic Materials,'' *J. Appl. Mech.*, **18**, 101–106 (1951).
7. I. Brazinsky, H. F. Cosway, C. F. Valle, Jr., R. Jones, R. Clark, and V. Story, ''A Theoretical Study of Liquid-film Spread Heights in the Calendering of Newtonian and Power Law Fluids,'' *J. Appl. Polym. Sci.*, **14**, 2771 (1970).
8. W. W. Alston and K. N. Astill, ''An Analysis of the Calendering of Non-Newtonian Fluids,'' *J. Appl. Polym. Sci.*, **17**, 3157 (1973).
9. P. R. Paslay, ''Calendering of Viscoelastic Materials,'' *J. Appl. Mech.*, **24**, 602 (1957).
10. N. Tokita and J. L. White, ''Milling Behavior of Gum Elastomers,'' *J. Appl. Polym. Sci.*, **10**, 1011 (1966).
11. J. S. Chong, ''Calendering Thermoplastic Materials,'' *J. Appl. Polym. Sci.*, **12**, 191–212 (1968).
12. J. F. Agassant and P. Avenas, ''Calendering of PVC—Forecast of Stresses and Torques,'' paper presented at the 2nd Int. Symp. on PVC, Lyon, France, 1976; also, J. L. Bourgeois and J. F. Agassant, ''Calendering of PVC—Defects in Calendered PVC Films and Sheets,'' paper presented at the 2nd Int. Symp. on PVC, Lyon, France, 1976.
13. J. L. White, ''Elastomer Rheology and Processing,'' *Rubber Chem. Technol.*, **42**, 257–338 (1969).
14. M. Finston, ''Thermal Effects in Calendering of Plastic Materials,'' *J. Appl. Mech.*, **18**, 12 (1951).
15. R. Takserman-Krozer, G. Schenkel, and G. Ehrmann, ''Fluid Flow between Rotating Cylinders,'' *Rheol. Acta*, **14**, 1066–1076 (1975).
16. N. G. Bekin, V. V. Litvinov, and V. Yu. Petrusanskii, ''Method of Calculation of the Energy and Hydrodynamic Characteristics of the Calendering of Polymeric Materails,'' *Kauch. Rezina*, **8**, 32 (1975); [English transl., *Int. Polym. Sci. Technol.*, **3**, T 55–T 58 (1976)].
17. C. Kiparissides and J. Vlachopoulos, ''Finite Element Analysis of Calendering,'' *Polym. Eng. Sci.*, **16**, 712 (1976).

18. R. V. Torner, ''Grundprozesse der Verarbeitung von Polymerer,'' VEB Deutscher Verlag für Grundstoffindustrie, Leipzig, 1974 (translated from Russian).
19. V. Yu. Petrusanskii and A. I. Stachaev, *Uch. Zap. Jaroslavsk. Technol. Inst.*, t. 23 (1971).
20. R. I. Tanner, ''Some Experiences Using Finite Element Methods in Polymer Processing and Rheology,'' *Proc. Seventh Int. Congr. on Rheology*, Gothenburg, Sweden, 1976, pp. 140–145.
21. J. Vlachopoulos and C. Kiparissides, ''An Analysis of Thermoplastics in Calendering,'' paper presented at the 26th Canadian Chemical Engineering Conf., Toronto, Canada, 1976.
22. C. Kiparissides and J. Vlachopoulos, ''A Study of Viscous Dissipation of Calendering of Power Law Fluids,'' *Polym. Eng. Sci.*, **18**, 210–213 (1978).
23. O. C. Zienkiewicz, *The Finite Element Method in Engineering Science*, McGraw-Hill, London, 1971.
24. J. N. Reddy and D. K. Gartling, *The Finite Element Method in Heat Transfer and Fluid Dynamics*, CRC Press, London, 2001.
25. K. H. Huebner, H. Dewhirst, D. L. Smith, and D. E. Byron, *Finite Element Method*, Wiley, New York, 2001.
26. J. Donea and A. Huerta, *Finite Element Methods for Flow Problems*, Wiley, Chichester, UK, 2002.
27. O. C. Zienkiewicz and C. Taylor, ''Weighted Residual Processes in Finite Elements with Particular Reference to Some Transient and Coupled Problems,'' in *Lectures on Finite Element Methods in Continuum Mechanics*, J. T. Oden and E. R. A. Oliveria, Eds., U. A. H. Press, Huntsville, AL, 1973.
28. J. T. Oden, O. C. Zienkiewicz, R. H. Gallagher, and C. Taylor, Eds., *Finite Elements in Flow Problems*, U. A. H. Press, Huntsville, AL, 1974, p. 4.
29. G. E. Myers, ''Finite Elements,'' in *Analytical Methods in Conduction Heat Transfer*, McGraw-Hill, New York, 1971, Chapter 9.
30. Z. Tadmor, E. Broyer, and C. Gutfinger, ''Flow Analysis Network (FAN), A Method for Solving Flow Problems in Polymer Processing,'' *Polym. Eng. Sci.*, **14**, 660–665 (1974).
31. C. S. Desai and J. F. Abel, *Introduction to the Finite Element Method—A Numerical Method for Engineering Analysis*, Van Nostrand Reinhold, New York, 1972, p. 68.
32. E. Broyer, C. Gutfinger, and Z. Tadmor, ''Evaluating Flows of a Non-Newtonian Fluid by the Method of Equivalent Newtonian Viscosity,'' *AIChE J.*, **21**, 198–200 (1975).
33. C. Gutfinger, E. Broyer, and Z. Tadmor, ''Analysis of a Cross Head Film Blowing Die with the Flow Analysis Network (FAN) Method,'' *Polym. Eng. Sci.*, **15**, 381–385 (1975).
34. E. Broyer, C. Gutfinger, and Z. Tadmor, ''A Theoretical Model for the Cavity Filling Process in Injection Molding,'' *Trans. Soc. Rheol.*, **19**, 423–444 (1975).
35. B. David, T. Sapir, A. Nir, and Z. Tadmor, ''Twin Rotor Mixers and Extruders, The Extended Cartesian Flow Analysis Network Method,'' *Int. Polym. Process.,* **5**, 155 (1990).
36. J. L. White, *Twin Screw Extrusion-Technology and Principles*, Hanser, Munich, 1990.
37. E. Mitsoulis, J. Vlachopoulos, and F. A. Mirza, ''Finite Element Analysis of Two-dimensional Polymer Melt Flows,'' *Polym. Process. Eng*., **1**, 283–308 (1983).
38. J. Vlachopoulos and A. N. Hrymak, ''Calendering of PVC: Theory and Experiments,'' *Polym. Eng. Sci.*, **20**, 725–731 (1980).
39. H. J. Park, D. Kim, K.-J. Lee, and E. Mitsoulis, ''Numerical Simulation in Converging Channel Flow of the Fluid M1 Using an Integral Constitutive Equation,'' *J. Non-Newt. Fluid Mech.*, **52**, 69–89 (1994).
40. X. L. Luo, ''A Control Volume Approach for Integral Viscoelastic Models and Its Application to Contraction Flow of Polymer Melts,'' *J. Non-Newt. Fluid Mech.*, **64**, 173–189 (1996).

41. D. Mewes, S. Luther, and K. Riest, ''Simultaneous Calculation of Roll Deformation and Polymer Flow in the Calendering Process,'' *Int. Polym. Process.*, **17**, 339–346 (2002).

42. A. C. Papanastasiou, L. E. Scriven, and C. W. Macosco, '' An Integral Constitutive Equation for Mixed Flows: Viscoelastic Characterization,'' *J. Rheol.*, **27**, 387–410 (1983).

43. D. Gross, W. Hauger, W. Schnell, and P. Wriggers, *Technische mechanic, Band 4*. Srpinger-Verlag, Berlin, 1999.

44. L. R. G. Treloar, *The Physics of Rubber Elasticity*, Clarendon Press, Oxford, 1975.

PROBLEMS

15.1 ***Calendering of Polymers: The Newtonian Gaskell Model*** A 0.2-m-diameter, 1-m-wide, equal-sized-roll calender operates at a speed of 50 cm/s. At a gap separation of 0.02 cm, it produces a 0.022-cm-thick film. Assuming a Newtonian viscosity of 10^4 poise, calculate in the last nip (a) the maximum pressure; (b) the separating force; and (c) estimate the mean temperature rise.

15.2 ***Separating Force between Rolls in an Experimental Calender*** A cellulose acetate–based polymeric compound is calendered on a laboratory inverted, L-shaped calender with 16-in-wide rolls of 8 in diameter. The minimum gap between the rolls is 15 mil. The sheet width is 15 in. Calculate the separation force and the maximum pressure between a pair of rolls as a function of exiting film thickness, assuming that film thickness equals the gap separation at the point of detachment. Both rolls turn at 10 rpm. The polymer at the calendered temperature of 90°C follows a Power Law model with $m = 3 \times 10^6$ dyne.s^n/cm^2 and $n = 0.5$. [Data based partly on J. S. Chong, ''Calendering Thermoplastic Materials,'' *J. Appl. Polym. Sci.*, **12**, 191–212 (1968).]

15.3 ***Design Considerations of a Calender*** We would like to manufacture a 2 m wide, 0.1 mm thick PVC film at a rate of 1200 kg/h with an inverted-L calender. Suggest a design procedure to select roll sizes, gap separations, and operating conditions.

15.4 ***Dissipated Work in Calendering*** Calculate the dissipated mechanical work during the forming of the sheet by calendering, as described in Problem 15.1. How much work would be dissipated if the sheet were extruded at the same rate through a sheet die with a 0.02-cm opening and 10-cm-long die lip.

15.5 ***FEM versus Analytical Solution of Flow in a Tapered Gap*** Consider isothermal pressure flow of a constant viscosity Newtonian fluid, between infinite plates, 10 cm long with a linearly decreasing gap size of 1.5 cm at the entrance and 1 cm at the exit. The distance between the entrance and the exit is 10 cm. The pressure at the inlet and outlet are 2 atmospheres and zero, respectively. (a) Calculate the pressure distribution invoking the lubrication approximation. (b) Calculate the pressure profile using the FEM formulation with six equal-sized elements, and compare the results to (a).